^{19}F spin-lattice relaxation in the cubic antiferromagnet $KNiF_3$

M. Engelsberg
Departamento de Física, Universidade Federal de Pernambuco, 50.000, Recife, Pernambuco, Brasil
(Received 21 September 1979)

The temperature dependence of the ^{19}F spin-lattice relaxation in the cubic quasi-isotropic antiferromagnet $KNiF_3$ is studied experimentally and theoretically. Quantitative agreement with measured relaxation rates is obtained over a considerable temperature range by assuming a two-magnon relaxation process in the "domain-flopped" state.

I. INTRODUCTION

The mechanisms of nuclear spin-lattice relaxation (NSLR) in antiferromagnetic insulators have been extensively studied both theoretically and experimentally over the last decade. Theoretical predictions[1,2] about the temperature dependence and field dependence of the spin-lattice relaxation time T_1 have been very accurately confirmed experimentally in the uniaxial antiferromagnets[3–5] MnF_2 and FeF_2. Another type of compound reasonably well understood as far as the proton NSLR is concerned is the family of hydrated halides of transition metals.[6] At present the central role of various scattering mechanisms involving magnons is well established and in many cases accounts quantitatively for the observed NSLR rates in various systems. It is then rather surprising to find that ^{19}F NSLR in the family of model antiferromagnets of the perovskite type, including $RbMnF_3$,[7,8] $KMnF_3$,[9] and $KNiF_3$,[10] appears to be rather poorly understood below the Néel temperature T_N. Except for $KMnF_3$, which exhibits structural phase transitions at low temperatures, the other two crystals are known to remain basically cubic at all temperatures. In addition to cubic symmetry, another distinctive characteristic shared by $KNiF_3$ and $RbMnF_3$ is that they are almost perfect Heisenberg antiferromagnets with very small relative anisotropy. The ratio H_A/H_E of anisotropy to exchange field has the value 7×10^{-5} for $KNiF_3$ and an even smaller value of 5×10^{-6} for $RbMnF_3$.

Of importance for the interpretation of the NSLR data in these systems is the fact that, unlike uniaxial antiferromagnets, cubic crystals lack a sharp "spin-flop" transition at a field $H_{cr}=(2H_AH_E+H_A^2)^{1/2}$. Instead, domain-wall movement takes place as the field is increased until a domain structure with the sublattice magnetization perpendicular to the applied field is attained. This "domain spin flop" may be completed[11–13] at fields well below H_{cr}.

In Sec. III of this paper the results of measurements of ^{19}F NSLR rates in $KNiF_3$ as a function of temperature are presented and the analysis of the data is discussed. In Sec. II a theoretical calculation of the temperature dependence of the relaxation rate is presented. The proposed relaxation mechanism is a two-magnon scattering process in the domain-flopped state accompanied by a nuclear spin flip via the F–Ni hyperfine interaction. Using a spherical approximation for the magnon dispersion relation, quantitative agreement with the measured relaxation rates was obtained over a considerable range of temperatures. A different and not yet understood relaxation mechanism appears to be effective at the lowest temperatures both in $KNiF_3$ and $RbMnF_3$.[7,8]

II. THEORY

A. Magnetic interactions in $KNiF_3$

Figure 1(a) shows a crystal unit cell of $KNiF_3$. Each Ni^{2+} ion is surrounded by six other Ni^{2+} ions in opposite sublattices and is coupled to them by an exchange interaction. With an external field $\vec{H}_0$ applied along [100] it becomes necessary to distinguish between two types of ^{19}F spins. $F_\parallel$ denotes ^{19}F spins whose bonds to its two-nearest neighboring Ni^{2+} ions are parallel to $\vec{H}_0$, whereas $F_\perp$ denotes the twice-as-abundant fluorines, whose bonds are perpendicular. In an applied field $H_0=7415$ Oe the resonances of both types of ^{19}F spins are separated by a splitting of 59 Oe, and perpendicular domains are known to prevail.[13]

Each fluorine spin interacts via a hyperfine coupling with two Ni^{2+} ions in different sublattices. Figure 1(b) shows a $F_\perp$ spin in a d_x-type domain where the sublattice magnetization is essentially along the x axis, although d_y-type domains are equally probable. The hyperfine coupling between the $F_\perp$ spin shown in Fig. 1(b) and its two neighboring Ni^{2+} ions can be written in the local $(\pi\pi'\sigma)$ coordinate system[14] in the form

$$\begin{aligned}\mathcal{H}_r = {} & A_\parallel I_{\sigma_1} S_{\sigma_1}(A) + A_\perp [I_{\pi_1'} S_{\pi_1'}(A) + I_{\pi_1} S_{\pi_1}(A)] \\ & + A_\parallel I_{\sigma_2} S_{\sigma_2}(B) \\ & + A_\perp [I_{\pi_2'} S_{\pi_2'}(B) + I_{\pi_2} S_{\pi_2}(B)] \ , \end{aligned} \tag{1}$$

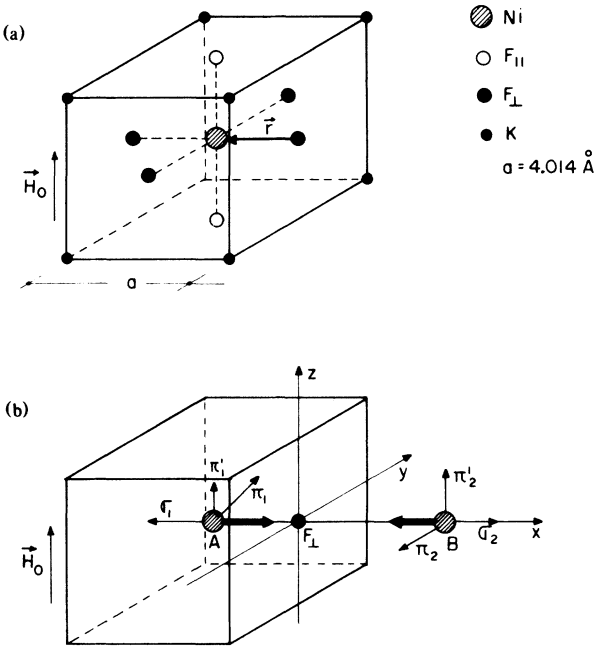

FIG. 1. (a) Crystal unit cell of $KNiF_3$. (b) $F_{\perp}$ nucleus with its two-nearest neighboring Ni^{2+} ions and coordinate system used in the text.

where $\vec{I}$ denotes the nuclear spin operator of the fluorine nucleus ($I=\frac{1}{2}$) and $\vec{S}(A)$, $\vec{S}(B)$ denote electron spins of the Ni^{2+} ions ($S=1$). The hyperfine coupling constants are well known experimentally[15] and have the values $A_{\parallel}=50.5\times10^{-4}$ cm^{-1} and $A_{\perp}=25.6\times10^{-4}$ cm^{-1}.

It is convenient to introduce new sets of coordinates[16] as shown in Fig. 2, such that the z' and z'' axes of the new sets are parallel to the slightly "canted" sublattice magnetizations. Transforming from the local coordinates to the "canted" coordinates yields

$$\begin{aligned}\mathcal{H}_r = A_{\parallel}I_x[&S_y''(B)\sin\theta + S_z''(B)\cos\theta \\ &- S_z'(A)\cos\theta - S_y'(A)\sin\theta] \\ &+ A_{\perp}I_y[S_x'(A) + S_x''(B)] \ ,\end{aligned} \tag{2}$$

where terms containing I_z have been dropped because they do not contribute to NSLR. Since the exchange field $H_E \simeq 3.6\times10^6$ Oe is much larger than the applied field the canting angle $\theta = \arcsin(H_0/2H_E)$ is very small. One is then allowed to neglect terms in $\sin\theta$ in Eq. (2) and set $\cos\theta \simeq 1$, obtaining

$$\begin{aligned}\mathcal{H}_r = A_{\parallel}I_x&[S_z''(B) - S_z'(A)] \\ &+ A_{\perp}I_y[S_x'(A) + S_x''(B)] \ .\end{aligned} \tag{3}$$

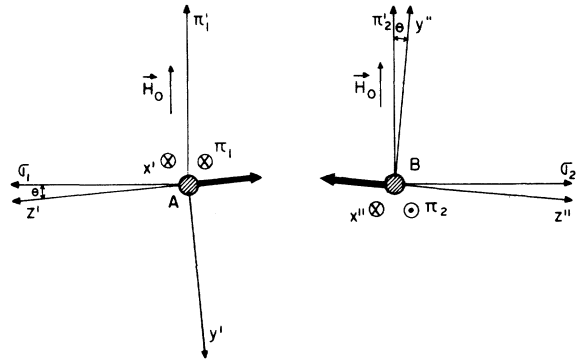

FIG. 2. Canted coordinate system. The z' and z'' axes are parallel to the sublattice magnetizations.

B. NSLR by a two-magnon scattering process

Spin deviation operators $a_j(A)$ and $a_j^{\dagger}(A)$ are introduced into the relaxation Hamiltonian $\mathcal{H}_r$ through the transformations

$$\begin{aligned}&S_{x'j}(A) + iS_{y'j}(A) = (2S)^{1/2}a_j(A) \ , \\ &S_{x'j}(A) - iS_{y'j}(A) = (2S)^{1/2}a_j^{\dagger}(A) \ , \\ &S_{z'j}(A) = S - a_j^{\dagger}(A)a_j(A) \ .\end{aligned} \tag{4}$$

Similarly the spin deviations localized on ions in the opposite sublattice are defined by

$$\begin{aligned}&S_{x''l}(B) + iS_{y''l}(B) = (2S)^{1/2}b_l(B) \ , \\ &S_{x''l}(B) - iS_{y''l}(B) = (2S)^{1/2}b_l^{\dagger}(B) \ , \\ &S_{z''l}(B) = S - b_l^{\dagger}(B)b_l(B) \ .\end{aligned} \tag{5}$$

Magnon operators $a_{\vec{k}}$, $b_{\vec{k}}$ are now introduced by a spatial Fourier transformation

$$\begin{aligned}a_j(A) &= \frac{1}{\sqrt{N}}\sum_{\vec{k}} e^{i\vec{k}\cdot\vec{r}_j(A)}a_{\vec{k}} \ , \\ b_l(B) &= \frac{1}{\sqrt{N}}\sum_{\vec{k}} e^{i\vec{k}\cdot\vec{r}_l(B)}b_{\vec{k}} \ .\end{aligned} \tag{6}$$

The magnetic lattice of $KNiF_3$ is fcc, and the primitive magnetic cell is a parallelepiped of volume $2a^3$ containing one Ni^{2+} ion of each sublattice. N in Eqs. (6) denotes the number of primitive cells, and the sum extends over $\vec{k}$ vectors of the first Brillouin zone of the bcc reciprocal lattice.

The electronic energy involving Zeeman, exchange, anisotropy, and hyperfine energies can be expressed in terms of magnon operators. Furthermore, in the case of $KNiF_3$ one can neglect hyperfine interactions between Ni electronic and nuclear spins because the natural abundance of Ni nuclei with nuclear spin different from zero is only 1.25%. Hinderks and

Richards[16] found a transformation giving the normal-mode operators $c_{\vec{k}}$, $d_{\vec{k}}$ from the previously defined magnon operators $a_{\vec{k}}$, $b_{\vec{k}}$. In terms of the normal-mode operators the electronic Hamiltonian becomes

$$\mathcal{H}_e=\hbar\sum_{\vec{k}}(\Omega_{1\vec{k}}c_{\vec{k}}^{\dagger}c_{\vec{k}}+\Omega_{2\vec{k}}d_{\vec{k}}^{\dagger}d_{\vec{k}}) \ , \tag{7}$$

where the eigenfrequencies for the two branches are given by

$$\begin{aligned}\Omega_{1\vec{k}}^2&=\gamma^2H_e^2(1-\gamma_{\vec{k}}^2)+\omega_{1A}^2+\gamma^2H_0^2 \ ,\\ \Omega_{2\vec{k}}^2&=\gamma^2H_e^2(1-\gamma_{\vec{k}}^2)+\omega_{2A}^2 \ .\end{aligned} \tag{8}$$

For the cubic lattice of Ni^{2+} ions in $KNiF_3$ (Fig. 1), $\gamma_{\vec{k}}$ in Eqs. (8) has the form

$$\gamma_{\vec{k}}=\tfrac{1}{3}(\cos k_x a+\cos k_y a+\cos k_z a) \ . \tag{9}$$

The frequencies ω_{1A} and ω_{2A} in Eqs. (8) are of the order $\gamma(2H_AH_E)^{1/2}$, and γ is the gyromagnetic factor of the magnetic ion.

The required transformation to the normal-mode operators is given in Ref. 16 and has the form

$$\begin{bmatrix}a_{\vec{k}}\\ a_{-\vec{k}}^{\dagger}\\ b_{\vec{k}}\\ b_{-\vec{k}}^{\dagger}\end{bmatrix}=\begin{bmatrix}\nu_{1\vec{k}} & -\nu_{1\vec{k}} & -\nu_{2\vec{k}} & -\nu_{2\vec{k}}\\ -\nu_{1\vec{k}} & \nu_{1\vec{k}} & -\nu_{2\vec{k}} & -\nu_{2\vec{k}}\\ \nu_{1\vec{k}} & -\nu_{1\vec{k}} & \nu_{2\vec{k}} & \nu_{2\vec{k}}\\ -\nu_{1\vec{k}} & \nu_{1\vec{k}} & \nu_{2\vec{k}} & \nu_{2\vec{k}}\end{bmatrix}\begin{bmatrix}c_{\vec{k}}\\ c_{-\vec{k}}^{\dagger}\\ d_{\vec{k}}\\ d_{-\vec{k}}^{\dagger}\end{bmatrix} \ , \tag{10}$$

where

$$\nu_{1\vec{k}}=\frac{1}{2}\left(\frac{\gamma H_e}{\Omega_{1\vec{k}}}\right)^{1/2} \ ; \quad \nu_{2\vec{k}}=\frac{1}{2}\left(\frac{\gamma H_e}{\Omega_{2\vec{k}}}\right)^{1/2} \ . \tag{11}$$

Since the term in Eq. (3) containing the operators $S_{x'}(A)$ and $S_{x''}(B)$ gives only rise to one-magnon processes which are inhibited by energy conservation, it can be ignored. The remaining term which is the effective two-magnon relaxation Hamiltonian $\mathcal{H}_{r2}$ can be written in the following form:

$$\mathcal{H}_{r2}=\tfrac{1}{2}A_{\parallel}I_{+}[S_{z''}(B)-S_{z'}(A)]+\text{H.c.} \ , \tag{12}$$

where

$$I_{+}=I_x+iI_y \ .$$

Substituting into Eq. (12) magnon operators through Eqs. (5) and (6) and normal-mode operators through Eqs. (10) and (11) yields

$$\mathcal{H}_{r2}=2iA_{\parallel}I_{+}N^{-1}\left(\sum_{\vec{k}\vec{k}'}\nu_{1\vec{k}}\nu_{1\vec{k}'}\sin[\vec{r}\cdot(\vec{k}-\vec{k}')]\,c_{\vec{k}}^{\dagger}c_{\vec{k}'}+\sum_{\vec{k}\vec{k}'}\nu_{2\vec{k}}\nu_{2\vec{k}'}\sin[\vec{r}\cdot(\vec{k}-\vec{k}')]\,d_{\vec{k}}^{\dagger}d_{\vec{k}'}\right)+\text{H.c.} \ , \tag{13}$$

where $\vec{r}$ is the $F_{\perp}$–Ni internuclear vector shown in Fig. 1(a). In Eq. (13) only processes involving creation and annihilation of normal-mode magnons in the same branch are included. Processes involving magnons in different branches are seen from Eqs. (8) to involve energy differences of at least order $\gamma\hbar H_0$, much larger than the nuclear Zeeman energy $\gamma_n\hbar H_0$. F–Ni magnetic dipole interactions make a relatively small contribution to the two-magnon relaxation rate and are also neglected.

Applying conventional first-order time-dependent perturbation theory,[2] the spin-lattice relaxation rate of the fluorine spin shown in Fig. 16 can be readily calculated.

Since the probabilities of the processes involving magnons in each branch can be considered to be additive, one has

$$\frac{1}{T_1}=\left(\frac{1}{T_1}\right)_1+\left(\frac{1}{T_1}\right)_2 \ , \tag{14}$$

where

$$\left(\frac{1}{T_1}\right)_i=\frac{16\pi A_{\parallel}^2}{\hbar N^2}\sum_{\vec{k}\vec{k}'}\nu_{i\vec{k}}\nu_{1\vec{k}'}\sin^2[\vec{r}\cdot(\vec{k}-\vec{k}')]\,\bar{n}_{i\vec{k}}(\bar{n}_{i\vec{k}'}+1)\delta(\hbar\Omega_{i\vec{k}}-\hbar\Omega_{i\vec{k}'}-\hbar\omega_n) \ ; \quad i=1,2. \tag{15}$$

$\bar{n}_{i\vec{k}}=1/[\exp(\hbar\Omega_{ik}/\kappa T)-1]$ in Eq. (15) is the Bose factor corresponding to a particular branch and $\omega_n=\gamma_nH_0$ is the nuclear angular frequency.

The relaxation rate given by Eq. (15) was derived for a particular fluorine nucleus of type $F_{\perp}$ [Fig. 1(b)]. For a fluorine of $F_{\parallel}$ type [Fig. 1(a)], a similar calculation leads simply to an exchange of $A_{\parallel}$ by $A_{\perp}$ in Eq. (15). Since the resonances of $F_{\perp}$ and $F_{\parallel}$ spins are partly overlapping, there exists the possibility of cross-relaxation effects, as will be discussed Sec. III. Moreover, the particular $F_{\perp}$ spin shown in Fig. 1(b) corresponds to a d_x-type domain and is charac-

terized by a F–Ni bond parallel to the sublattice magnetization. The same $F_\perp$ spin in a d_y-type domain or an adjacent $F_\perp$ spin in a d_x-type domain would have its F–Ni bond directed perpendicular to the sublattice magnetization and would relax at a rate proportional to $A_\perp^2$. However, since the resonances of these two types of $F_\perp$ spins completely overlap,[13] a common spin temperature is established in a very short time of the order of T_2, and the system can be assumed to relax at the fastest of both rates which is governed by $A_\parallel^2 = 3.85 A_\perp^2$.

C. Spherical approximation

In the spherical approximation,[4,5] the exact magnon dispersion relations Eqs. (8) and (9) are substituted by approximate expressions depending only upon $|\vec{k}|$. This has the great mathematical advantage of allowing one to transform the sums in Eq. (15) into integrals over a spherical Brillouin zone and still retain some realistic details such as a peak in the magnon density of states. It is expected that a spherical approximation should be more appropriate in a cubic crystal with only a single exchange constant like $KNiF_3$ or $RbMnF_3$ than in MnF_2. In fact the exact density of states in MnF_2 for $\vec{k} \| (100)$ has two peaks rather than one, and this has been shown[5] to cause some additional discrepancies with the predictions of a spherical model.

The application of the spherical approximation to the $KNiF_3$ lattice involves the substitution of the exact Brillouin zone, a truncated octahedron of volume $4(\pi/a)^3$ by a spherical Brillouin zone of radius $k_{\max} = \sqrt{3}\pi/2a$. Both surfaces are tangent along [111] directions. Since the total volume of the spherical Brillouin zone is smaller than the correct value by a factor $8/\sqrt{3}\pi$, we adopt the procedure of Butler *et al.*[4] of distributing uniformly the "missing" states. This conserves the total number of modes but introduces an error in the density of states for small $\vec{k}$ which is increased from the exact value by a factor $8/\sqrt{3}\pi$.

The sperical approximation on the dispersion relations consists of replacing $\gamma_{\vec{k}}$ given by Eq. (9) by

$$\gamma_k = \cos(ka/\sqrt{3}) \quad . \tag{16}$$

As k is varied from $k=0$ to $k_{\max} = \sqrt{3}\pi/2a$, the approximate eigenfrequencies resulting from Eqs. (8) by using γ_k in Eq. (16) change from the exact minimum values to the exact maximum values. Moreover, the exact dispersion relations coincide with the approximate ones for $\vec{k}_\parallel [111]$.

Conservation of the total number of modes dictates that the following substitution be made in Eq. (15)

$$\frac{1}{N}\sum_{\vec{k}} \rightarrow \frac{1}{4/3\pi k_{\max}^3}\int_0^{k_{\max}} d^3k \quad . \tag{17}$$

This allows one to reduce Eq. (15) after some manipulation to a one-dimensional integral over frequencies of form

$$\left[\frac{1}{T_1}\right]_i = \frac{512 A_\parallel^2 a^6}{3\hbar^2\pi^5}\int_{\omega_{im}}^{\Omega_{iM}} \frac{\nu_{ik}^4 k^4(\bar{n}_{ik}+1)\bar{n}_{ik}[1-(\sin ka/ka)^2]d\Omega_{ik}}{(d\Omega_{ik}/dk)(d\Omega_{ik'}/dk')_{\Omega_{ik'}(n)}} \quad , \quad i=1,2, \quad \Omega_{ik'}(n) = \Omega_{ik} - \omega_n \quad . \tag{18}$$

where the minimum and maximum frequencies ω_{im} and Ω_{iM} obtained from Eqs. (8) are given by

$$\begin{aligned} \Omega_{1M} &= (\gamma^2 H_e^2 + \omega_{1A}^2 + \gamma^2 H_0^2)^{1/2} \quad , \\ \omega_{1m} &= (\omega_{1A}^2 + \gamma^2 H_0^2)^{1/2} \quad , \\ \Omega_{2M} &= (\gamma^2 H_e^2 + \omega_{2A}^2)^{1/2}, \quad \omega_{2m} = \omega_{2A} \quad . \end{aligned} \tag{19}$$

The nuclear angular frequency ω_n appearing in the δ function of Eq. (15) has little effect and can be neglected in most terms appearing in Eq. (18). In the term

$$\left[\frac{d\Omega_{ik'}}{dk'}\right]_{\Omega_{ik'}(n)(=\Omega_{ik}-\omega_n)} \quad ,$$

however, it must be taken into account to have a convegent integral in the full frequency interval including the maximum frequency Ω_{iM}.

III. EXPERIMENTAL RESULTS AND DISCUSSION

A. NSLR measurements in $KNiF_3$

^{19}F spin-lattice relaxation measurements were performed at 30 MHz using a conventional pulsed NMR spectrometer. The crystal was aligned with a [100] axis parallel to the external field and mounted at the end of the cold finger of a closed-cycle refrigerator cryostat.[17] In the range $250\ \text{K} \leq T \leq 33\ \text{K}$, T_1 varied over four orders of magnitude but at lower temperatures T_1 appears to be much more slowly varying. The dominant relaxation mechanisms in this low-temperature region, however, is not well understood at present.

The analysis of the data requires some care because of the presence of two slightly overlapping resonances corresponding to $F_\parallel$ and $F_\perp$ spins [Fig. 1(a)].

The spin-lattice relaxation time is measured by applying a sequence of four saturating 90° pulses at the resonance frequency of the more abundant $F_\perp$ spins and measuring the recovery of the magnetization. The radio-frequency pulses, however, also nutate partially the $F_\parallel$ magnetization. Figure 3 shows the recovery of the magnetization after a series of waiting times following saturation. The periodic pattern observed on the free-induction-decay (FID) signals has a period of 4.5 μsec corresponding to the expected[13] splitting $\Delta H = 59$ Oe at a frequency of 30 MHz.

Denoting by $S_\perp(\tau,t)$ the measured signal amplitude (Fig. 3) and assuming identical line shapes for the resonances of both types of fluorine spins, a simple analysis yields

$$S_\perp(\tau,t) = g(\tau)[M_\perp(t) + (1-f^2)^{1/2} M_\parallel(t) \times \cos(\gamma_n \Delta H \tau)] \ , \quad (20)$$

where $g(\tau)$ represents the decay of the transverse component of magnetization for either type of fluorine and $M_\perp(t)$, $M_\parallel(t)$ denote longitudinal components of magnetization at time t after saturation. Assuming that the cross-relaxation[18] rate ν is much smaller that the spin-lattice relaxation rates, each type of fluorine spin relaxes independently. Thus

$$M_\perp(t) = M_0(1 - e^{-\nu_\perp t}) \ , \quad (21)$$

$$M_\parallel(t) = \tfrac{1}{2} M_0[1 - (1-f^n)e^{-\nu_\parallel t}] \ , \quad (22)$$

where f in Eqs. (20) and (22) denotes the fraction of $F_\parallel$ equilibrium magnetization $\frac{1}{2}M_0$ remaining along the z axis after applying a single 90° pulse at the resonance frequency of the $F_\perp$ spins, the number of saturating 90° pulses is denoted by n in Eq. (22) and $\nu_\perp = (1/T_1)_\perp$, $\nu_\parallel = (1/T_1)_\parallel$. The signal amplitude $S_\perp(\tau_0 t)$ at time $\tau_0 = 2\pi/\gamma_n \Delta H$ (Fig. 3) obtained from

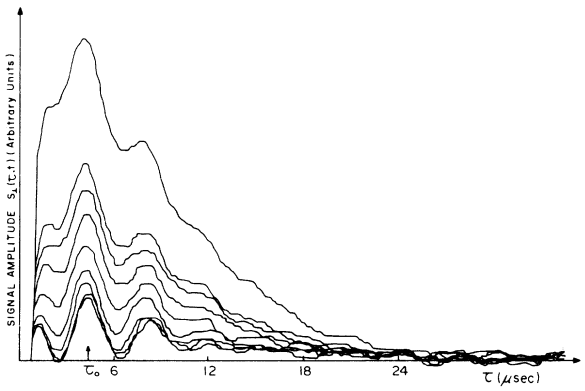

FIG. 3. ^{19}F magnetization recovery at various times following saturation. The top and bottom traces correspond to $t = \infty$ and 0, respectively.

Eqs. (20)–(22) is given by

$$\frac{S_\perp(\tau_0\infty) - S_\perp(\tau_0 t)}{S_\perp(\tau_0\infty)} = \frac{e^{-\nu_\perp t} + \frac{1}{2}(1-f^2)^{1/2}(1-f^n)e^{-\nu_\parallel t}}{1 + \frac{1}{2}(-f^2)^{1/2}} \ . \quad (23)$$

The numerical value of f can be obtained empirically from the expression

$$\frac{S_\perp(\tau_0\infty) - S_\perp(\tau_0 0)}{S_\perp(\tau_0\infty)} = \frac{1 + \frac{1}{2}(1-f^2)^{1/2}(1-f^n)}{1 + \frac{1}{2}(1-f^2)^{1/2}} \ ,$$

resulting from Eq. (23) and from the data shown in Fig. 3. It can also be obtained from the shape of the decay through Eq. (20). For $n = 4$ both methods yield approximately coincident values of $f \simeq 0.9$. Substitution of this value of f into Eq. (23) yields

$$[S_\perp(\tau_0,\infty) - S_\perp(\tau_0,t)]/S_\perp(\tau_0\infty) = 0.82e^{-\nu_\perp t} - 0.061e^{-\nu_\parallel t} \ . \quad (24)$$

The second term on the right side of Eq. (24) only amounts to a small correction and the recovery of the $F_\perp$ magnetization is expected to follow a single exponential with time constant $(T_1)_\perp = 1/\nu_\perp$.

At sufficiently low temperatures, the temperature-independent cross-relaxation rate ν may become comparable with the spin-lattice relaxation rates $\nu_\parallel$ and $\nu_\perp$ and should be taken into account. One can attempt to estimate the cross-relaxation rate ν from the overlap[18] between the resonances of $F_\perp$ and $F_\parallel$ spins, although this overlap is known to be extremely sensitive to the details of the wings of the resonance line shapes. For that purpose it was assumed that both resonances corresponding to $F_\perp$ and $F_\parallel$ spins had identical shapes and a single fitting function centered at each resonance was used to numerically compute the normalized overlap. The Fourier transform of the fitting function[19,20] used was of the type $g(\tau) = \exp\{C[A - (A^2+\tau^2)^{1/2}]\}$, where the parameters C and A were determined from the observable part of the FID signals. The value of the overlap obtained in this manner was of order 10^{-6}. Since one expects[18] ν to be smaller than $1/T_2 \approx 10^5$ sec^{-1} by a factor of the order of the overlap, the value of the cross-relaxation rate can be estimated to be $\nu \approx 0.1$ sec^{-1}. Such a value of ν would justify the assumption implicit in Eqs. (21) and (22) in the temperature range 250 K $\lesssim T \lesssim$ 33 K and would explain the single-exponential time dependencies observed.

B. Discussion

Figure 4 shows a plot of the logarithm of the measured relaxation rate $(1/T_1)_\perp$ as a function of inverse

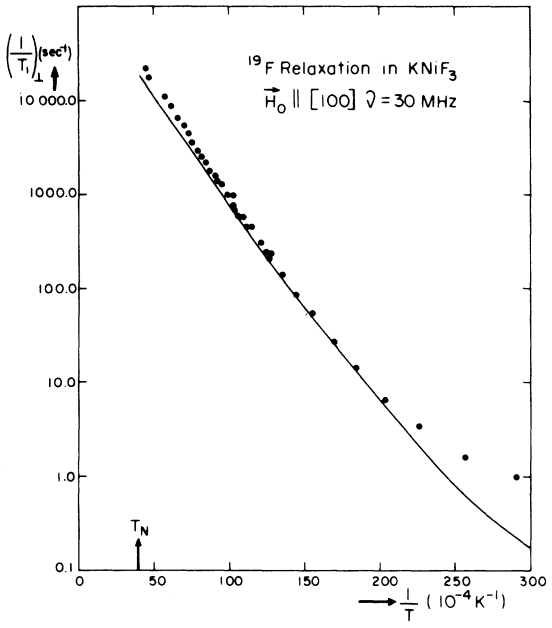

FIG. 4. The logarithm of the ^{19}F NSLR rate as a function of inverse temperature. The circles are experimental points and the solid line is the calculate two-magnon relaxation rate.

temperature. Also shown in Fig. 4 is the result of the numerical integration of Eq. (18). The numerical values of the parameters used in the calculation of the theoretical relaxation rate were $A_{\parallel} = 50.5 \times 10^{-4}$ cm^{-1},[15] $\hbar\Omega_{1M} = \hbar\Omega_{2M} = 356$ cm^{-1}. This last value is somewhat smaller but within the experimental error of the value 373 ± 17 cm^{-1} obtained from the exchange constant quoted by Lines.[21] The adopted values of the lower limits of the integrals were[22] $\omega_{2m} = 4.5$ cm^{-1} and $\omega_{1m} = 4$, 6 cm^{-1}. This difference between the minimum frequencies in the magnon spectrum of the two branches is caused by the external magnetic field $H_0 = 7415$ Oe. Its influence upon the calculated relaxation rates, however, is negligible in the temperatuare range of the measurements shown in Fig. 4. Thus both branches contribute equally to the calculated rates and no field dependence is expected. Also negligible is the field dependence introduced by the δ function in Eq. (15).

The good agreement between theory and experiment strongly suggests that in the temperature range considered a two-magnon scattering mechanism is responsible for the observed NSLR rates in the "domain-flopped" state. It is expected that the same mechanism will quantitatively explain the higher-temperature field-independent ^{19}F NSLR mechanism in $RbMnF_3$ (Refs. 7 and 8). One can also conclude from the results presented that the applicability of the spherical approximation is not limited to relatively dispersionless antiferromagnets as was suggested in Ref. 4.

It is somewhat intriguing the relatively small departure of the experimental data shown in Fig. 4 from the predictions of noninteracting spin-wave theory at the higher temperatures. This suggests the magnon-magnon interactions in this system would play a comparatively minor role in the ^{19}F NSLR even relatively close to T_N. A more careful theoretical analysis would be needed to further clarify this point.

ACKNOWLEDGMENTS

We wish to thank Dr. P. A. Fleury of Bell Laboratories for kindly providing the $KNiF_3$ crystal and Professor S. M. Rezende, Professor E. A. Soares, and Professor B. Žekš for useful discussions. This work was supported by the Conselho Nacional de Desenvolvimento Cientifico e Tecnológico, Financiadoro de Estudos e Projetos (FINEP), (Brazilian Agencies) and OEA (Organizacão dos Estados Americanos).

[1]T. Moriya, Prog. Theor. Phys. (Kyoto) 16, 23 (1956).
[2]D. Beeman and D. Pincus, Phys. Rev. 166, 359 (1968).
[3]N. Kaplan, R. Loudon, V. Jaccarino, H. J. Guggenheim, D. Beeman, and P. A. Pincus, Phys. Rev. Lett. 17, 357 (1966).
[4]M. Butler, Tin Ngwe, N. Kaplan, and H. J. Guggenheim, Phys. Rev. 185, 816 (1969).
[5]D. Paquette, A. R. King, and V. Jaccarino, Phys. Rev. B 11, 1193 (1975).
[6]I. J. Lowe and D. W. Whitson, Phys. Rev. B 6, 3262 (1972).
[7]L. L. Hess and E. R. Hunt, Phys. Rev. B 6, 45 (1972).
[8]E. R. Hunt and T. Horiguchi, Phys. Rev. B 11, 1804 (1975).
[9]R. J. Mahler, A. C. Daniel, and P. T. Parrish, Phys. Rev. Lett. 19, 85 (1967).
[10]M. Engelsberg, S. M. Rezende, and E. A. Soares, J. Appl. Phys. 50, 1929 (1979).
[11]R. H. Petit, J. Ferré, and J. Nouet, J. Phys. (Paris) 36, 431 (1975).
[12]M. Safa and B. K. Tanner, Philos. Mag. B 37, 739 (1978).
[13]M. Engelsberg, Phys. Rev. B (in press).
[14]E. A. Turov and M. Petrov, *Nuclear Magnetic Resonance in Ferro and Antiferromagnets* (Halstedt, New York, 1972), Chap. VIII.
[15]R. G. Shulman and S. Sugano, Phys. Rev. 130, 506 (1963).
[16]Larry W. Hinderks and Peter M. Richards, Phys. Rev. 183, 575 (1969).

[17]Displex, Air Products and Chemicals Inc., Allentown, Pennsylvania 18103.
[18]N. Bloembergen, S. Shapiro, P. S. Pershan, and J. O. Artman, Phys. Rev. 114, 445 (1959).
[19]D. A. McArthur, E. L. Hahn, and R. E. Walstedt, Phys. Rev. 188, 609 (1969).
[20]M. Engelsberg and I. J. Lowe, Phys. Rev. 10, 822 (1974).
[21]M. E. Lines, Phys. Rev. 164, 736 (1967).
[22]P. Moch and C. Dugathier, in *Proceedings of the International Conference in Magnetism, Moscow, 1973* (Nauka, Moscow, 1974), Vol. I, p. 185.